Rock Mech Rock Eng (2017) 50:1863–1882
DOI 10.1007/s00603-017-1188-0

ORIGINAL PAPER

Role of Brittle Behaviour of Soft Calcarenites Under Low Confinement: Laboratory Observations and Numerical Investigation

Piernicola Lollino[1] · **Gioacchino Francesco Andriani**[2]

Received: 6 June 2016 / Accepted: 18 February 2017 / Published online: 28 February 2017

Abstract The strength decay that occurs in the post-peak stage, under low confinement stress, represents a key factor of the stress–strain behaviour of rocks. However, for soft rocks this issue is generally underestimated or even neglected in the solution of boundary value problems, as for example those concerning the stability of underground cavities or rocky cliffs. In these cases, the constitutive models frequently used in limit equilibrium analyses or more sophisticated numerical calculations are, respectively, rigid-plastic or elastic–perfectly plastic. In particular, most of commercial continuum-based numerical codes propose a variety of constitutive models, including elasticity, elasto-plasticity, strain-softening and elasto-viscoplasticity, which are not exhaustive in simulating the progressive failure mechanisms affecting brittle rock materials, these being characterized by material detachment and crack opening and propagation. As a consequence, a numerical coupling with mechanical joint propagation is needed to cope with fracture mechanics. Therefore, continuum-based applications that treat the simulation of the failure processes of intact rock masses at low stress levels may need the adoption of numerical techniques capable of implementing fracture mechanics and rock brittleness concepts, as it is shown in this paper. This work is aimed at highlighting, for some applications of rock mechanics, the essential role of post-peak brittleness of soft rocks by means of the application of a hybrid finite–discrete element method. This method allows for a proper simulation of the brittle rock behaviour and the related mechanism of fracture propagation. In particular, the paper presents two ideal problems, represented by a shallow underground cave and a vertical cliff, for which the evolution of the stability conditions is investigated by comparing the solutions obtained implementing different brittle material responses with those resulting from the assumption of perfectly plastic behaviour. To this purpose, a series of petrophysical and mechanical tests were conducted on samples of soft calcarenite belonging to the Calcarenite di Gravina Fm. (Apulia, Southern Italy), focusing specific attention on the post-peak behaviour of the material under three types of loading (compression, indirect tension and shear). Typical geometrical features representative of real rock engineering problems observed in Southern Italy were assumed in the problems examined. The numerical results indicate the impact of soft rock brittleness in the assessment of stability and highlight the need for the adoption of innovative numerical techniques to analyse these types of problems properly.

Keywords Soft calcarenite · Brittleness · Hybrid FDEM technique · Rock stability

1 Introduction

The stability of rock masses in different rock mechanics applications, from slopes to underground caves, can be treated nowadays by using a wide range of calculation tools that range from simple limit equilibrium techniques to sophisticated coupled finite/distinct element codes. However, it is worthwhile pointing out that for the great majority of the commercial codes these stability problems

✉ Piernicola Lollino
p.lollino@ba.irpi.cnr.it

[1] CNR, Istituto di Ricerca per la Protezione Idrogeologica, Bari, Italy

[2] Dipartimento di Scienze della Terra e Geoambientali, Università degli Studi di Bari Aldo Moro, Bari, Italy

are dealt with by adopting perfect plasticity to simulate intact rock behaviour. This is generally true both for limit analysis and limit equilibrium analysis approaches, which assume rigid-plastic rock behaviour accounting for either Mohr–Coulomb or Hoek–Brown failure criterion (Gesualdo et al. 2001; Fraldi and Guarracino 2009, 2010; Suchowerska et al. 2012). Recently, more sophisticated numerical modelling approaches, using the continuum-based finite element method (FEM), were adopted to investigate intact rock and rock mass behaviour, from soft to hard rock (Hammah et al. 2008; Ferrero et al. 2010; Parise and Lollino 2011; Suchowerska et al. 2012; Ciantia et al. 2015). FEM technique is generally considered as the most widespread numerical tool, due to its robustness in dealing with material inhomogeneity, nonlinearity, complex three-dimensional geometries, soil–structure interactions and the availability of well-verified commercial codes. In FEM models, the choice of using elastic–perfectly plastic models also for brittle materials frequently arises also from the need to reduce numerical problems related to loss of uniqueness and mesh dependency of the solution associated with the use of strain-softening models, unless more sophisticated techniques are introduced to regularize the solution (de Borst et al. 1993; Borja et al. 2000; Di Prisco et al. 2002; Troncone 2005). A review of numerical techniques used in rock slope stability analysis, with recent developments in the application of continuum and discontinuum numerical codes, is proposed by Stead et al. (2006). With regard to the assessment of stability of underground cavities, Parise and Lollino (2011), Lollino et al. (2013), Ferrero et al. (2010), Suchowerska et al. (2012) and Ciantia and Castellanza (2016), just to mention few examples, apply the elastic–perfectly plastic model, using either the Mohr–Coulomb or the Hoek–Brown failure criterion, to simulate the behaviour of intact rock masses surrounding the cavities examined.

However, the assumption of perfect plasticity for those rock materials that show a pronounced post-failure brittle behaviour, along with the choice of the peak strength as the representative material strength, can lead to an overestimation of the rock strength and the stability of the system at the scale of the boundary value problem, and in some cases also to an inadequate understanding of the failure mechanisms. In fact, most rock types exhibit a brittle response in the post-failure stage of the stress–strain curve, especially at low confinement, and therefore numerical models dealing with stability problems at low confining stress cannot ignore this issue. From an historical point of view, the post-peak behaviour of rocks has been studied only after the adoption of stiff servo-controlled test machines in the mid-1960s (Hudson et al. 1972). Various attempts were made in the last decades to develop theories capable of properly describing rock brittleness. Hajiabdolmajid et al. (2002) remark that perfectly plastic models are not appropriate to simulate the behaviour of brittle rocks and adopt a cohesion-weakening frictional strength model, for which the strength decay from peak to residual is strain dependent. Martin (1997) demonstrates that the brittle rock failure is a gradual process of cohesive strength weakening by tensile cracking at the early stages of loading, while mobilization of the frictional strength component actually occurs when the cohesive strength component is significantly reduced. Diederichs (2003) points out that the brittle behaviour of rock begins when the stress–strain state reaches the damage threshold, i.e. before peak strength, when rock starts to break according to individual fractures that become axial splitting, normal to the direction of the minimum principal stress. This brittle behaviour is particularly prominent at low confining stresses, where failure is dominated by extensile cracking and propagation of tensile fractures. However, this process is not observed in the laboratory and, as a consequence, the in situ failure envelope is supposed to be even lower than that measured in the laboratory, especially near excavation boundaries (Ghazvinian et al. 2013; Cai and Kaiser 2014). Kaiser and Kim (2015) remark that brittle rocks fail by extensional crack damage leading to spalling at low confinement and to shear-band formation at high confinement, so that two different brittle failure modes, i.e. extension fracture and proper shear failure mode, should be considered depending on the stress level. The same Authors also remark that the standard failure criteria, i.e. Mohr–Coulomb or Hoek–Brown, although considering the effect of confinement, implicitly assume shear failure mode, with an instantaneous mobilization of both the cohesive and the frictional strength, without explicitly taking into account the change in the physical process between extensional cracking and shear failure modes. It follows that the classic failure criteria implicitly assume that the shear mode, and not spalling, is the predominant failure mechanism, independent of the actual confinement. Based on the previous considerations, the mobilization of strength in brittle failure of rock can be schematized according to a two-stage process, with a pre-peak stage controlled mainly by cohesive force and a post-peak strength dominated by frictional strength. Recent studies have proposed methods to evaluate rock brittleness parameters from uniaxial and triaxial compression tests (Meng et al. 2015), along with cohesive fracture models for soft rocks (Gui et al. 2015).

Concerning rock mechanics applications, Kaiser and Kim (2008) emphasize that rock brittleness should be accounted for in the interpretation of laboratory test data as well as in analytical or numerical design tools. In general, to deal with brittle rock failure in a simplified way, two different sets of parameters, respectively, representative of the peak and post-peak rock strength envelopes, are proposed in the literature. In particular, the post-peak strength

envelope should be characterized by a very small post-peak cohesion and a friction angle which reflects the frictional strength of fractured rocks under low confinements. Carranza-Torres et al. (2002) propose a solution to quantify the drop of strength in terms of the Mohr–Coulomb yield criterion, from the peak to residual condition, by means of a "strength loss" parameter, which controls the slope of the softening branch of the stress–strain curve. Cundall et al. (2003) present another model based on the Hoek–Brown failure criterion that essentially incorporates a three-part plasticity flow rule that varies as a function of the confining stress. Golchinfar (2013) shows the results of simulating brittle rock failure near an excavation boundary by using an instantaneous strength mobilization model ("the brittle Mohr–Coulomb model"), which is characterized by an instantaneous cohesion loss, from peak to post-peak strength, and an instantaneous friction mobilization, from initial to post-peak friction angle. As a more sophisticated alternative, the cohesion-weakening and friction-strengthening (CWFS) model, which is based on a multi-line failure criterion, is well-recognized and widely used to simulate the brittle rock failure (Vasak and Kaiser 1995; Hajiabdolmajid et al. 2002; Cheon et al. 2006; Diederichs 2007; Edelbro 2010; Zhao et al. 2010). However, such continuum modelling approaches are based on classical shear failure theory for elasto-plastic materials, but a number of experimental observations demonstrate that the use of discontinuum modelling approaches is more appropriate for brittle spalling processes in rock masses under low confinement conditions, such as those characterizing the near-field of excavations.

To this aim, the hybrid FDEM approach combines aspects of both finite elements and discrete elements with fracture mechanics principles. The finite-element-based analysis of continua is merged with discrete-element-based transient dynamics, contact detection and contact interaction solutions (Munjiza 2004). As a consequence, it is capable of simulating the real stress–strain curve of the rock material, so that, using the fracture mechanics principles, it can comply with both the extension fracture and the shear failure mode. In this perspective, such a numerical method is promising for the realistic simulation of brittle-fracture-driven processes of rock and a full consideration of the failure kinematics at the rock mass scale. Several applications of the FDEM technique have been carried out to study rock failure problems, including rock slope failure analysis (Stead et al. 2004; Eberhardt et al. 2004) or mine pillars (Pine et al. 2006; Elmo and Stead 2010). The FDEM technique has also been recently implemented in Irazu software (Geomechanica Inc 2016) and used to develop insights into the fracturing behaviour of rocks (Mahabadi et al. 2012; Lisjak et al. 2014; Tatone and Grasselli 2015).

The purpose of this paper is to characterize the post-failure behaviour of a soft calcarenite, belonging to the Calcarenite di Gravina Fm. (Apulia, Southern Italy), as observed from laboratory testing. Afterwards, the effects of simulating the observed rock brittleness for two ideal stability problems, i.e. the stability of a rectangular underground cave and that of a vertical cliff, are dealt with. The material studied is a Plio-Pleistocene highly porous calcarenite, which in outcrop exposures is massive and rather homogeneous, in terms of textural and structural characters (Andriani and Walsh 2002). Therefore, the results of petrographical and mechanical testing and analysis are firstly presented. Later on, the results of numerical analyses performed by means of advanced FDEM hybrid techniques (Geomechanica Inc 2016), allowing for a proper simulation of the post-peak stress–strain behaviour, are proposed and compared with conventional FEM approaches in the framework of perfectly plastic model behaviour. The role of treating the brittle behaviour of intact rock with a proper numerical technique in boundary value problems is therefore discussed to gain new insight into the failure process of the examined geomaterial.

2 Rock Material Characterization

2.1 Petrographical Features and Microstructural Fabric

A soft rock variety belonging to the Calcarenite di Gravina Fm. (upper Pliocene–lower Pleistocene), a thin formation (lower than 70–100 m in thickness) cropping out on the eastern margin of the Bradanic Trough and on the flanks of the Murge plateaux, from the present-day sea level up to more than 400 m in elevation (Azzaroli 1968; Iannone and Pieri 1979), was assumed in this study as representative to highlight the typical mechanical behaviour of the soft rocks belonging to the aforementioned geological formation. However, it is worthwhile pointing out that throughout the region the rock material belonging to the Calcarenite di Gravina Fm. exhibits spatial (both horizontal and vertical) variability according to different facies distributions as a consequence of a complex depositional history. The Calcarenite di Gravina Fm. consists of transgressive shallow-marine carbonates, composed of bioclasts and terrigenous limestone fragments, which unconformably overlie up to 3-km-thick Mesozoic–Cenozoic faulted limestone successions belonging to the Apulian carbonate platform (Pomar and Tropeano 2001 and references therein).

Intact blocks of this calcarenite were selected from "Papapietro" quarry at Montescaglioso, an important rock exploitation site in Basilicata (southern Italy) (Fig. 1). This quarry is located in the south margin of the Matera Horst,

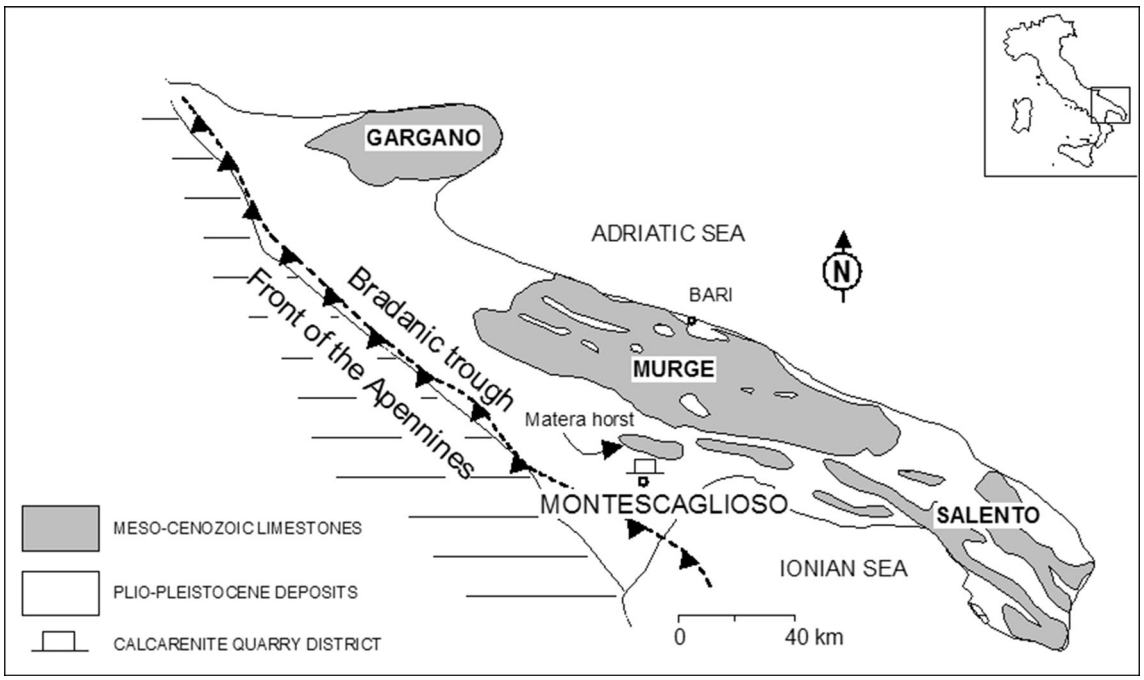

Fig. 1 Location of the study area

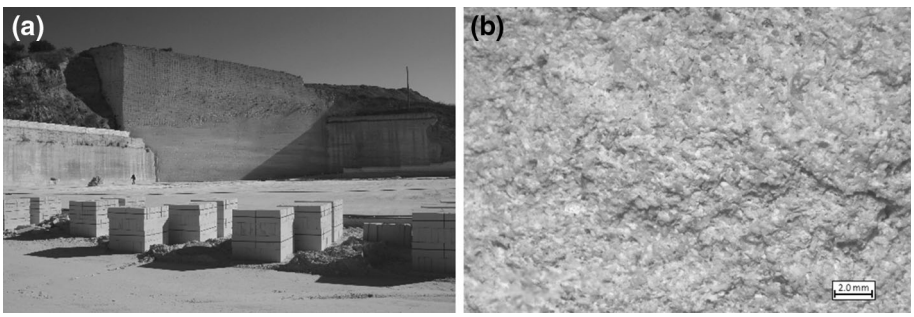

Fig. 2 **a** View of the open pit walls, "Papapietro" Quarry, Montescaglioso (southern Italy); **b** macrophotographs from a coarse-grained packstone specimen used for testing

on the south-western part of the Murge area (Mateu-Vicens et al. 2008). Here, the calcarenites are generally well sorted and coarse grained, but exhibit a finer grading upward. They are also massive and rather homogeneous, with no macroscopic internal structures, except for rare faults and a subtle stratification, resulting from occasional thin beds of fine carbonate gravels (Fig. 2a). The calcarenites are poorly and irregularly cemented, light yellow coloured and composed of low-magnesium calcite (98%), with an insoluble residue of mainly clay minerals and negligible presence of quartz, feldspars, gibbsite and goethite.

Rock fabric inspection was performed by means of transmitted light on standard thin sections using optical polarizing microscopy. The granular framework is mainly formed by a bioclast fraction, represented by dermal plates and prickles of echinoids, benthic foraminifers, encrusting colonies of bryozoans, balanis, calcareous algae, and lamellibranchs and gastropods in fragments above all. Bioclasts exhibit micrite envelopes in places, while microboring is common especially in coarse bivalves. Lithoclasts include sub-rounded fragments of whitish calcilutites and dolomitic limestone, derived from the erosion of the Mesozoic basement. Fabric is open and typical of grain-supported biolithoclastic calcarenites, mainly biosparites and also biosparmicrites, the latter being generally found in the upper layers of the deposit (Fig. 2b). In particular, the texture of calcarenites consisting of shell fragments and, subordinately, lithoclasts, along with sparry calcite cement (biosparites), can be classified as "grainstone" according to Dunham (1962), whereas calcarenites consisting of shell fragments along with a silty–muddy matrix cemented mainly by an initial finely bladed crust (biosparmicrites) can be classified as "packstone" (Dunham 1962) (Fig. 3). The packing degree is low, so that the diagenesis of these calcarenite sediments is likely to have occurred soon after deposition. Therefore, precipitation of

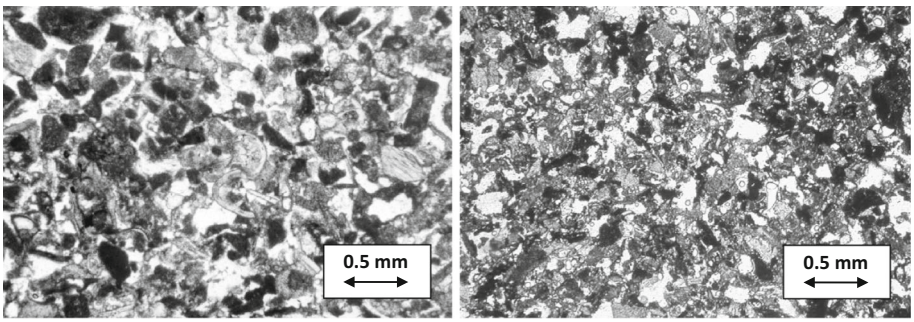

Fig. 3 Images of photographic thin sections in plane-polarized light. On the *right*, the packstone facies; on the *left*, the grainstone facies

Table 1 Physical and mechanical properties of the calcarenite rocks from "Papapietro" Quarry, Montescaglioso (southern Italy)

Physical–mechanical properties	Packstone	Grainstone
Specific gravity, G_s	2.70	2.70
Dry unit weight, γ_d (kN/m^3)	13.54–14.13	13.64–15.30
Saturated unit weight, γ_{sat} (kN/m^3)	17.46–18.74	17.66–18.93
Porosity, n (%)	44–48	42–47
Degree of saturation, S_r (%)	100	100
Compr. strength (dry), σ_{cdry} (MPa)	4.1–4.9	4.3–5.6
Compr. strength (sat), σ_{csat} (MPa)	2.3–3.4	2.6–3.8
Indir. tensile strength (dry), σ_{tBdry} (MPa)	0.45–0.56	0.51–0.61
Indir. tensile strength (sat), σ_{tBsat} (MPa)	0.26–0.32	0.31–0.42

cement took place in the initial phases of compaction or even before experiencing increments of pressure and temperature due to burial. Not surprisingly, the lithofacies studied show meniscus calcitic cement (early-stage cement) at grain contacts in many places. This is accompanied by a border of finely crystalline calcite on the grain external surfaces, covered only in some places by lengthened crystals and microcrystals with a scalenohedronic or rhombohedral form (dog tooth cement). Late stage cement (sparry calcite), which partially or totally filled pore spaces, is uncommon, although it is not easy to distinguish between fine sparry cement, recrystallization and neomorphic microspar. The lithofacies described above is characterized by open porosity, so that all the pores are interconnected and accessible. According to the pore type and porosity classification of carbonate rocks proposed by Choquette and Pray (1970), the main contribution to the total porosity is provided by the primary intergranular porosity, which is followed, in order of priority, by the intragranular porosity, moldic porosity and fracture porosity on a microscopic and mesoscopic scale.

2.2 Physical and Mechanical Properties

Following the standard test procedures proposed by ISRM (1979a, b), dry unit weight (γ_d) and total porosity (n) were determined on about 100 cylindrical samples (72 mm in diameter) of calcarenite (Table 1). To this purpose, a specific gravity (G_s) of 2.7 was assumed on the basis of the mineralogical composition of the lithofacies examined.

Afterwards, according to Andriani and Walsh (2003, 2007), water absorption (w_a) and degree of saturation (S_r) were estimated on specimens submerged for 48 h in distilled water at 20 °C and then saturated completely under vacuum (80 kPa). Following this procedure, a saturation degree approximately equal to 100% was obtained for the samples; this means that porosity of these calcarenites can be considered as open (effective porosity). Grain size analysis was also carried out; in order to obtain loose material for mechanical sieving method, a representative sample of saturated calcarenite was subjected to a large number of freeze–thaw cycles and then disaggregated by hand. The loose material obtained was dried at 105 °C for 24 h and, afterwards, sieved using aperture sizes ranging from 2.00 to 0.063 mm. The remaining fine fraction (passing 230, ASTM series) was subjected to sedimentation analysis. The resulting grain size curves are reported in Fig. 4. According to the classification of the Apulian calcarenites proposed by Andriani and Walsh (2010), the lithofacies here studied can be classified as "AC3", i.e. very soft coarse-grained calcarenite, with a grainstone or packstone texture, respectively, for the material cropping out in the lower and in the higher part of the quarry faces.

Uniaxial compressive strength and indirect tensile strength (Brazilian) tests, under both dry (σ_{cdry}, σ_{tdry}) and

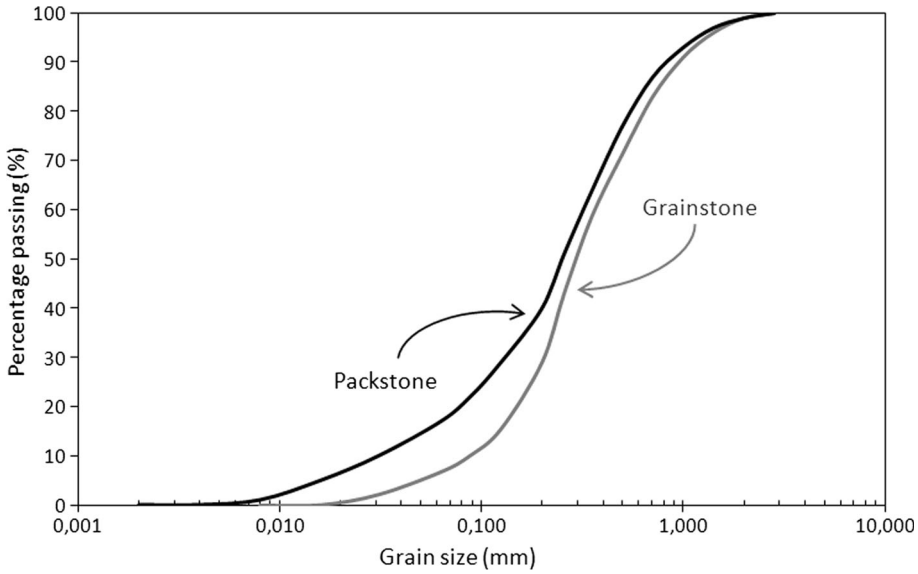

Fig. 4 Grain size distribution curves obtained using sieve and sedimentation analysis

saturated state (σ_{csat}, σ_{tsat}), were carried out according to ISRM (1978, 1979b). The post-peak behaviour of the rock material was observed during the tests by using a servo-controlled testing machine. From this point of view, it is worthwhile pointing out that the post-peak response of the rock can depend also on the specimen geometry (Hudson 2014). The results of the mechanical test here presented (Table 1) were also compared with those obtained for similar rock materials by Castellanza and Nova (2004), Andriani and Walsh (2010) and Ciantia et al. (2015).

The uniaxial compressive strength (UCS) performed on dry samples of the Montescaglioso calcarenite ranges between 4.0 and 5.5 MPa, with the lowest values typically found for the packstone lithofacies. For saturated calcarenite, UCS decreases about 35% on average, with strength reductions from dry to wet material generally ranging between 25 and 50% and the largest reductions observed for the packstone levels. UCS values lower than those above indicated, even equal or lower than 1 MPa, have been also measured on wet calcarenite samples taken from different areas of the same geological region. The tensile strength obtained by means of the Brazilian test - method varies from 0.45 to 0.60 MPa for dry samples. For saturated material, the tensile strength decreases of about 40%, on average, and reaches lower values, even equal to 0.2 MPa, for different varieties of the same formation outcropping in the region. As already observed for the compressive strength, the lowest values of the tensile strength were obtained for the packstone samples. Therefore, it can be summarized that the mechanical behaviour of these calcarenites is strongly affected by the presence of water in the intergranular pores (Andriani and Walsh 2007, 2010; Ciantia et al. 2015), with the packstone facies more susceptible to the effect of saturation.

Figure 5 shows typical stress–strain curves obtained for the packstone and grainstone calcarenites here examined under uniaxial compression tests (a) and Brazilian tests (b). The post-peak behaviour of the calcarenites under study is comparable to that described by Wawersik and Fairhurst (1970) for the "stable" type of rock behaviour (class I). For this type of post-failure response of the rock, characterized by a "stable" fracture propagation, work must be done on the specimen for each incremental decrease in load-carrying ability. In this case, after the elastic portion, the stress–strain curves show a clear slope decrease associated with microfracturing activity and failure, where the stress exhibits a strong drop, related to the coalescence of microfractures and the development of roughly vertical cracks within the samples. The ultimate uniaxial compressive strength, i.e. at large uniaxial compressive strains, generally reaches values lower than 1.0–2.0 MPa. The values of fracture energy release, i.e. the amount of energy released during the strength decay from peak state to residual, as measured from uniaxial compression and indirect tensile tests, i.e. the area underlying the brittle portion of the stress–strain curves resulting from the same tests, which do not represent estimates of pure Mode I G_{If} energy fracture, can be identified in the range from 50 to 1000 N/m and from 20 to 100 N/m, respectively. The test results indicate that, both under uniaxial compression and indirect tensile tests, axial fracturing generally initiates at about 60% of the peak strength and develops firstly at the boundaries of the sample and then propagates towards the inner portions.

A mention should be made on the stress–strain curves that exhibit ductile behaviour of the material; as a matter of fact, this response is observed to be a typical feature of the calcarenites belonging to the packstone type only, when they are saturated (Fig. 6). This type of behaviour is

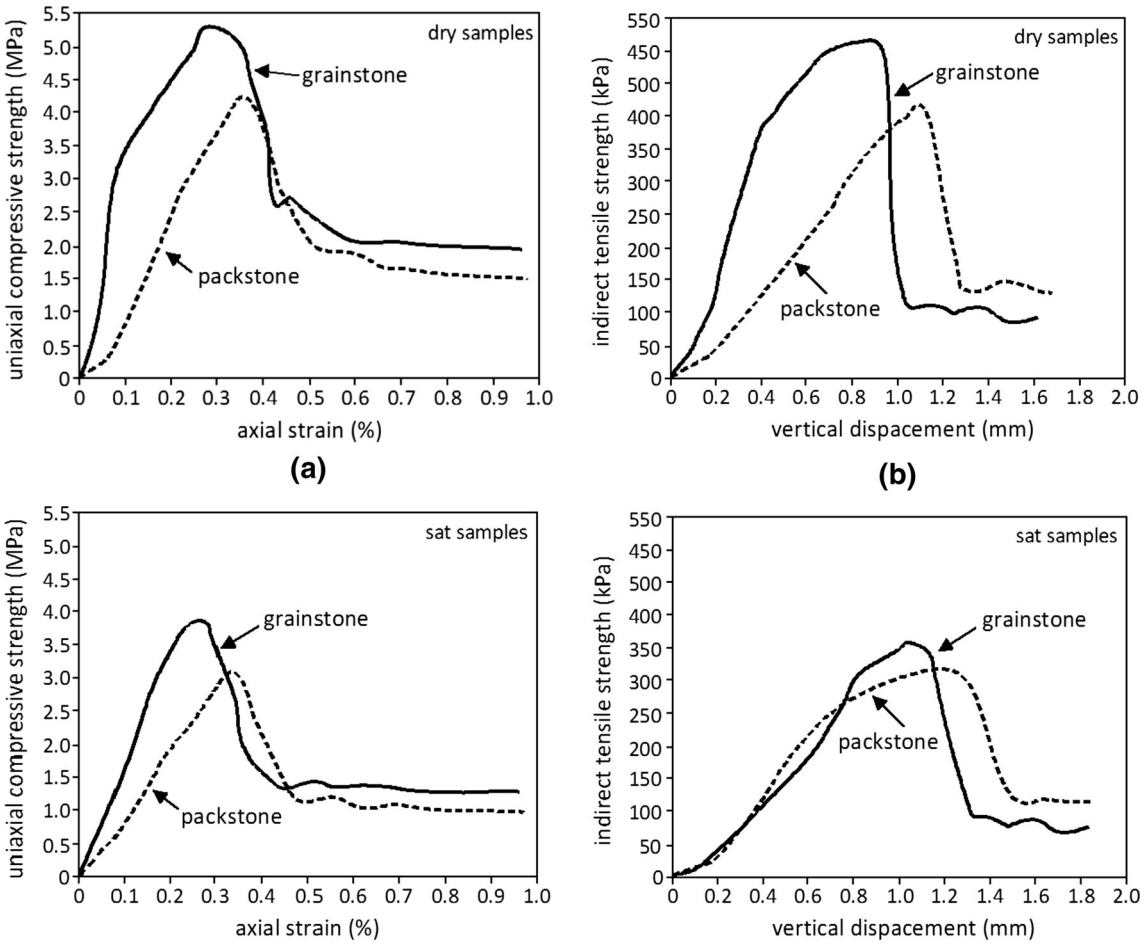

Fig. 5 Typical stress–strain curves obtained for servo-controlled uniaxial compression tests (**a**) and Brazilian tests (**b**) on the calcarenites under study

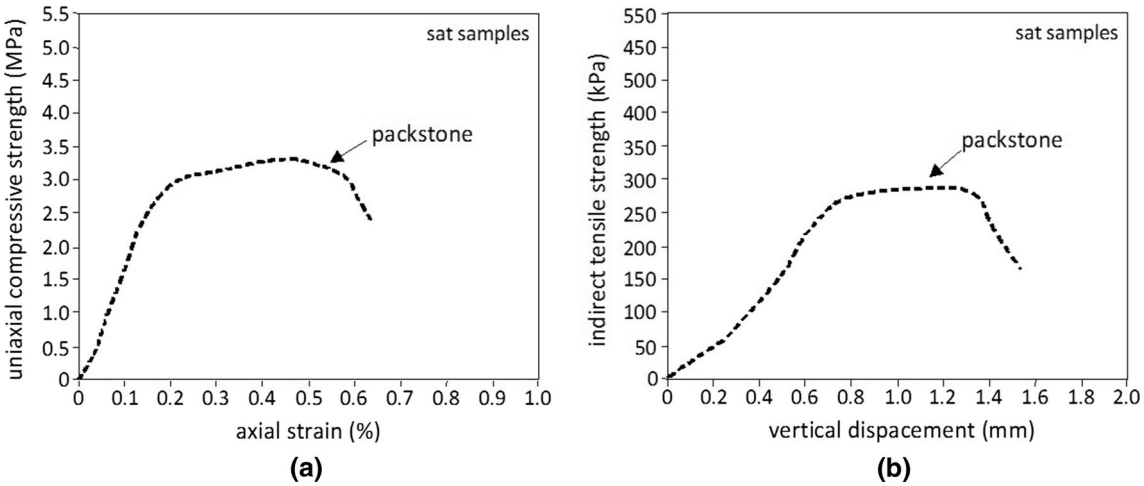

Fig. 6 Stress–strain curves showing ductile behaviour for servo-controlled uniaxial compression tests (**a**) and Brazilian tests (**b**) on some saturated samples belonging to the packstone facies

supposed to be related to the extremely irregular and variable distribution of cement, which is much more common where recrystallization has not taken place or is not complete. In the specific case of the "Papapietro" quarry, this occurs where the packstone type crops out, i.e. in the higher part of the quarry faces.

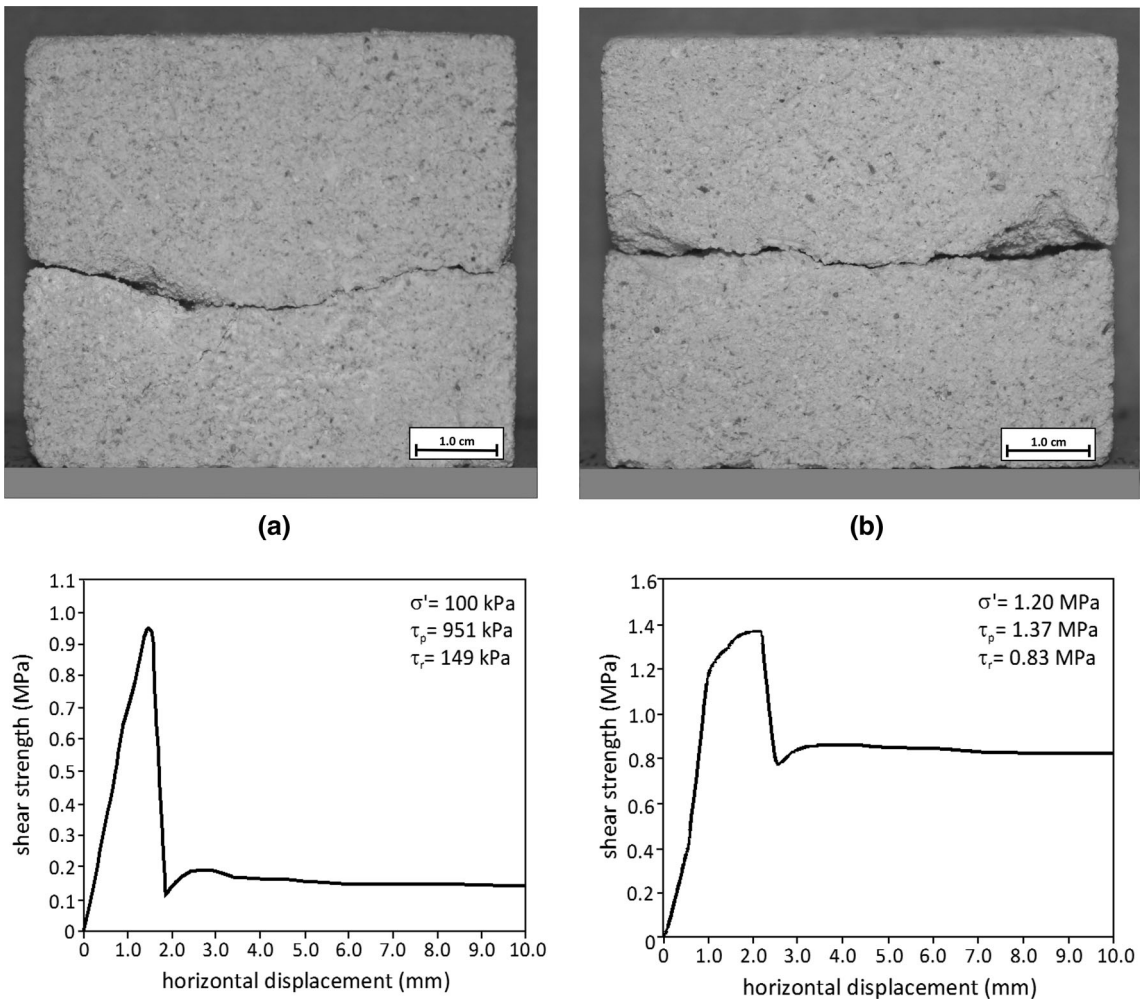

Fig. 7 Waviness and roughness of the shear surfaces and shear versus horizontal displacement curves obtained by means of direct shear tests on calcarenite samples with no existing joints at low (**a**) and high (**b**) effective normal stresses

Constant-rate direct shear tests were also carried out on intact calcarenite samples with no existing joints by means of a 60 × 60 × 50 mm square direct shear box according to ASTM D 3080-04. A displacement rate of 0.1 mm/min was chosen to guarantee drainage of pore water from the saturated samples during shearing. The shear tests were conducted under effective normal stresses between 5.0 kPa and 1.25 MPa. As regards the shear behaviour of the calcarenite here examined, no distinction was made in this study between the two textural types, packstone and grainstone. However, it is worthwhile pointing out that such a topic can be of high interest for a future investigation. The shear stress–horizontal displacement curves generally exhibit a clear brittle behaviour, after an initial elastic response, a yield stage immediately before that peak is reached and a failure stage corresponding to the peak of the curve. Just after the peak, the strength of the rock samples abruptly decreases due to the propagation of the shear-loading induced fracture along the pre-imposed shear plane (Fig. 7). The post-peak region is characterized by a first stage for which the effects of dilatancy due to the irregularities of the shear plane are evident and a residual stage when undulation and asperities are overcome or sheared off. The experimental data show that shearing smooths the failure surface for normal stress larger than or equal to 1.0 MPa, while under lower normal stresses the samples at the end of the test exhibit surfaces that are undulated and rough (Andriani and Walsh 1998). Within the range of the normal stress investigated, the peak shear strength (τ_{peak}) ranges between 0.87 and 1.73 MPa, while the residual values (τ_{res}) range between 73 kPa and 1.01 MPa (Fig. 7). As a consequence, a brittleness index considering a shear-dominant failure [$I_{\tau b} = (\tau_{peak} - \tau_{res})/\tau_{peak}$, Bishop 1967] in the range between 0.41 and 0.95 was identified for such material. A clear dependency of the brittle response with the confining stress is also generally observed. In fact, a more pronounced brittle behaviour occurs when the normal stress is lower than 450 kPa and

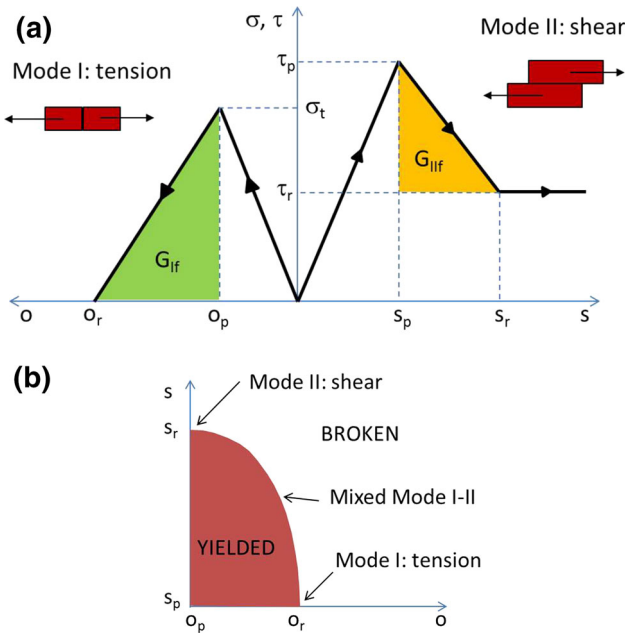

Fig. 8 **a** Schematic constitutive behaviour assumed for Mode I (opening) and Mode II (slip) fracture formation and propagation and related brittleness parameters, G_{If} and G_{IIf}; **b** elliptical coupling relationship between tensile opening and shear displacement, for mixed-mode fracturing (modified after Lisjak et al. 2014)

reduces at higher vertical stress values. According to the direct shear test results, the values of fracture energy for Mode II, G_{IIf}, i.e. the amount of energy released during the strength decay from peak state to residual and the consequent creation of a shear fracture (Lisjak et al. 2014), which is represented in this case by the area underlying the brittle portion of the stress–displacement curves under shear states (Fig. 8a), is observed in the range between 100 and 500 N/m.

3 The Hybrid FDEM Numerical Method

In order to overcome the limitations posed by the applicability of continuum-based models to address rock engineering problems that involve fracture and fragmentation processes, Munjiza (2004) first proposed the idea of using a new hybrid finite–discrete element method (FDEM). In this approach, the overall modelling domain is discretized into discrete elements, which are separated by crack elements and are internally divided into finite elements. Therefore, continuum behaviour is modelled through finite elements, while discontinuum behaviour is analysed by discrete elements and transition from continua to discontinua is simulated through fracture and fragmentation processes according to the main principles of nonlinear elastic fracture mechanics. As such, under Mode I (direct tension) the stress–strain curve of a rock is simulated by means of a pre-peak elastic portion, followed by the post-peak strain-softening behaviour, which is formulated in terms of a stress–displacement law of a single crack model undergoing tension (Fig. 8a). Similarly, the stress–strain curve under Mode II (shear behaviour) is simulated by means of an elastic behaviour and a post-peak portion, represented by a stress–displacement law of a crack model undergoing slip weakening (Fig. 8a). Therefore, material starts to yield, in tension or shear mode, upon reaching a displacement value corresponding to the maximum cohesive strength. The Mode I peak strength is defined by a constant tensile strength, σ_t, while the Mode II peak strength, τ_p, is computed according to the Mohr–Coulomb criterion ($\tau_p = c + \sigma_n \tan\phi_i$), where c is the cohesion, ϕ_i is the internal friction angle and σ_n is the normal stress acting across the crack element. When residual conditions are reached ($\tau = \tau_r$), a physical discontinuity is formed and the available shear strength is provided by a purely frictional strength ($\tau_r = \sigma_n \tan\phi_f$), with the friction angle equal to that available along the fracture, ϕ_f. Mixed Mode I–II crack initiation and propagation is also possible for intermediate stress states (Fig. 8b). Further details can be found in Munjiza (2004) and Lisjak et al. (2014).

In the hybrid continuum/discontinuum technique, the simulation starts with a continuum approach, typically through explicit integration of the equations of motion, until discontinuities are allowed to form when the failure envelope is reached along the mesh element boundaries. At this point, discrete element integration techniques are used for detecting new contacts and solving the interaction between discrete bodies, while FEM techniques are applied for detecting the eventual creation of new cracks. Fracture formation and propagation within the continuum is simulated by the breakage of the cohesive elements only along the boundaries of the triangular elements (Munjiza et al. 1999), so that the fracture trajectories are conditioned by the constraints imposed by the initial mesh adopted. Consequently, a sufficiently small element size should be adopted to reproduce the correct mechanical response (Munjiza and John 2002). The complete breakage of the crack element, and thus the nucleation of a discrete crack, is accomplished once the material fracture energy release rate, G_f, is completely dissipated; at this stage, the crack element is removed from the simulation and therefore the model transition from continuum to discontinuum is locally completed.

The FDEM modelling platform adopted for the numerical simulations here proposed is Irazu software (Geomechanica Inc 2016). In Irazu, the modelling domain is discretized with a mesh consisting of three-node triangular elements with four-node interface (or crack) elements embedded between the edges of adjacent triangle pairs (Fig. 9a). The progressive failure of rocks is simulated

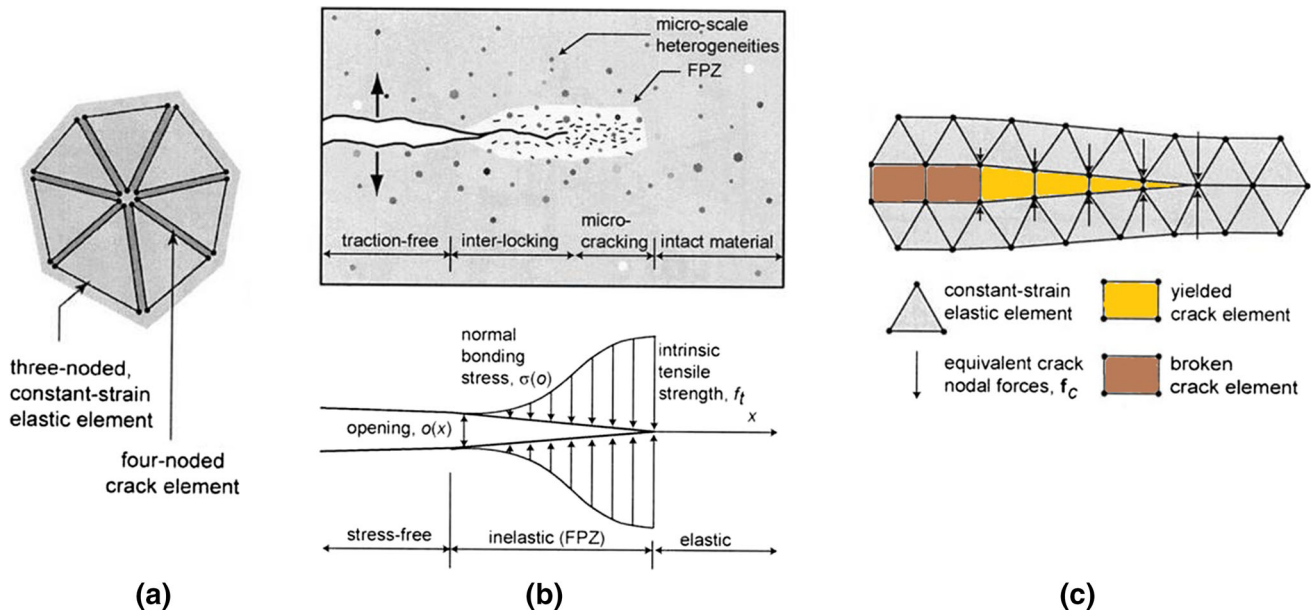

Fig. 9 Irazu numerical technique for the simulation of fracturing propagation (Lisjak et al. 2014): **a** schematic representation of a continuum using cohesive crack elements interposed among triangular elastic elements; **b** scheme of fracture propagation zone (FPZ) in brittle geomaterials (modified after Labuz et al. 1985) and theoretical FPZ model based on cohesive zone approach (modified after Hillerborg et al. 1976); **c** numerical representation of theoretical FPZ model in Irazu FDEM (Lisjak et al. 2014)

using a cohesive zone approach (Fig. 9b, after Hillerborg et al. 1976). During elastic loading, stresses and strains follow a linear elastic continuum model. Upon exceeding the peak strength of the material (in tension, shear or a mixed mode), the strains are assumed to localize within a narrow zone, known as the fracture process zone (Fig. 9b). In particular, when yield strength is reached, crack elements start to open or slip, with equivalent nodal forces representative of the interlocking effects, but when residual opening, o_r, or residual slippage, s_r, is attained, complete breakage of the crack element is assumed, with the formation of a stress-free surface or a shear fracture (Fig. 9c). The constitutive response of a crack element is defined in terms of the variation of the bonding stresses, σ and τ, between the edges of the triangular element pair as a function of the crack relative displacements, o and s, in the normal and tangential directions, respectively. In tension (i.e. Mode I), the response of each crack element depends on the Mode I fracture energy, G_{If}. In shear (i.e. Mode II), the post-peak behaviour is governed by the Mode II fracture energy, G_{IIf}. The Mode I and Mode II fracture energies, G_{If} and G_{IIf}, represent the amount of energy, per unit crack length along the crack edge, dissipated during the creation of a tensile and shear fracture and are, respectively, equal to the area below the post-peak portion of the curves in Fig. 8a, given by:

$$G_{If} = \int s(o)\mathrm{d}o \tag{1}$$

$$G_{IIf} = \int [t(s) - tr]\mathrm{d}s \tag{2}$$

For mixed Mode I–II fracturing, an elliptical coupling relationship is adopted between crack opening, o, and slip, s (Fig. 8b).

4 Effects of Brittleness of Soft Calcarenites on Stability Problems

Representative ideal rock engineering problems are proposed in this section in order to show the effects of accounting for brittleness and fragmentation processes of soft calcarenites by means of the hybrid FDEM approach, as compared with conventional finite element (FEM) models implementing perfect plasticity. In particular, numerical applications regarding the stability of two shallow underground cavities with rectangular cross section, characterized by different geometry, and that of a vertical slope face have been performed. The three applications were carried out by considering representative mechanical properties of calcarenite varieties belonging to the Calcarenite di Gravina Fm. The material parameters used in the numerical analyses here presented are reported in Table 2. In particular, conventional finite element analyses were firstly carried out with PLAXIS-2D by using an elastic–perfectly plastic constitutive model with a Mohr–Coulomb failure criterion and a tension cut-off. Three

Table 2 Material parameters used in the stability analysis

Parameter	γ (kN/m^3)	E' (MPa)	v	C' (kPa)	ϕ' (°)	σ_t (kPa)
Set 1	16.00	100	0.30	200	30	240
Set 2	16.00	100	0.30	200	30	180
Set 3	16.00	100	0.30	60	30	50

different sets of parameters representative of different strength conditions for the calcarenite under study, i.e. cohesion equal to $c' = 200$ kPa and tension strength equal to $\sigma_t = 240$ kPa (*Set 1*), $c' = 200$ kPa and $\sigma_t = 180$ kPa (*Set 2*) as well as cohesion $c' = 60$ kPa and tension strength $\sigma_t = 50$ kPa (*Set 3*, Table 2), with all of these sets assuming a friction angle constant equal to $\phi' = 30°$ and a dilation angle equal to $\psi = 0°$, have been assumed in the analyses below described, in accordance with the results of uniaxial compression, direct shear and indirect tension tests performed on samples belonging to different varieties of Calcarenite di Gravina. A Young's modulus equal to $E' = 100$ MPa and a Poisson ratio of $v = 0.30$ have been also adopted for all sets of material parameters on the basis of uniaxial compression test results. The corresponding FDEM analyses have adopted the same strength parameters used for the FEM simulations, whereas the fragility parameters, i.e. the Mode I G_{If} and Mode II G_{IIf} fracture energy values (Fig. 8a), have been estimated according to both the laboratory observations and the empirical relationships available in the specific literature. In particular, the Mode II G_{IIf} value has been derived from the results of the direct shear tests in terms of energy fracture release after that the maximum strength has been reached (see Sect. 2.2, Lisjak et al. 2014). In particular, based on the test results, this parameter results to be in the range between 100 and 500 N/m, with an average value approximately equal to $G_{IIf} = 200$ N/m. Then, the Mode I G_{If} value can be supposed in the range 10–50 N/m and equal to $G_{If} = 20$ N/m on average, if a ratio between Mode I and Mode II fracture energy parameters equal to $G_{If} \cong G_{IIf}/10$ is assumed (Lisjak et al. 2014).

Furthermore, since no direct tensile test was available on such a material, the empirical relationship proposed by Zhang (2002) has been also adopted in order to estimate G_{If}, as follows:

$$K_{IC} = s_t/6.88$$

where K_{IC} is the fracture toughness and σ_t is the tensile strength, and then G_{If} has been derived as:

$$G_{If} = K_{IC}^2/E'$$

where $E' = E/(1 - v^2)$, with $E =$ Young's modulus of the rock.

According to this approach, G_{If} results to be equal to 11 N/m for $\sigma_t = 240$ kPa and equal to 6 N/m for $\sigma_t = 180$ kPa ($E = 100$ MPa, $v = 0.3$), these values being considered as representative of the lower values of the corresponding range. It comes out that the most likely values of G_{If} lie in the range 10–50 N/m, with an average value approximately equal to $G_{If} = 20$ N/m. Based on the K_{IC} value above defined, the G_{IIf} energy release values derived from the laboratory observations also result to be in agreement with those estimated by assuming the values of the ratio between K_{IC} and K_{IIC} proposed by Backers and Stephansson (2012).

In order to calibrate both the rock strength values and the fragility parameters above defined, uniaxial compression and Brazilian tests have been simulated with the FDEM numerical technique by using *Set 1* strength data in Table 2 and $G_{If} = 20$ N/m–$G_{IIf} = 200$ N/m fragility parameters, and the results have been compared with the corresponding laboratory tests performed on Calcarenite di Gravina samples; moreover, for the case of the uniaxial compression test, a comparison with a FEM analysis adopting perfect plasticity for the rock has been also carried out. In particular, the results of both FDEM and FEM uniaxial compression test simulations along with the corresponding laboratory test results are reported in Fig. 10a in terms of axial stress (σ_a) against axial strain (ε_a), whereas the vertical displacements at failure resulting from the FDEM test simulation are shown in Fig. 10b. Figure 10a shows an acceptable agreement between the FDEM model and the laboratory test data in terms of both the maximum strength and the post-peak decay of the curve, with a slightly higher brittleness observed in the laboratory test. A value of the uniaxial compressive strength slightly lower than that predicted by the FDEM model is instead obtained from the FEM analysis. Figure 11a instead shows a comparison between the FDEM-based indirect tensile test simulation and the corresponding laboratory data in terms of indirect tensile stress against vertical displacement, whereas the FDEM failure mechanism typically observed in the Brazilian test is shown in Fig. 11b in terms of vertical displacements calculated at failure. Figure 11a indicates a satisfying agreement between the model results and the laboratory data in terms of pre-peak behaviour, indirect tensile strength as well as brittle response.

Based on such a calibration of both the rock strength data and the fragility parameters, the numerical simulations of the three rock engineering applications are presented below. These are engineering applications highly

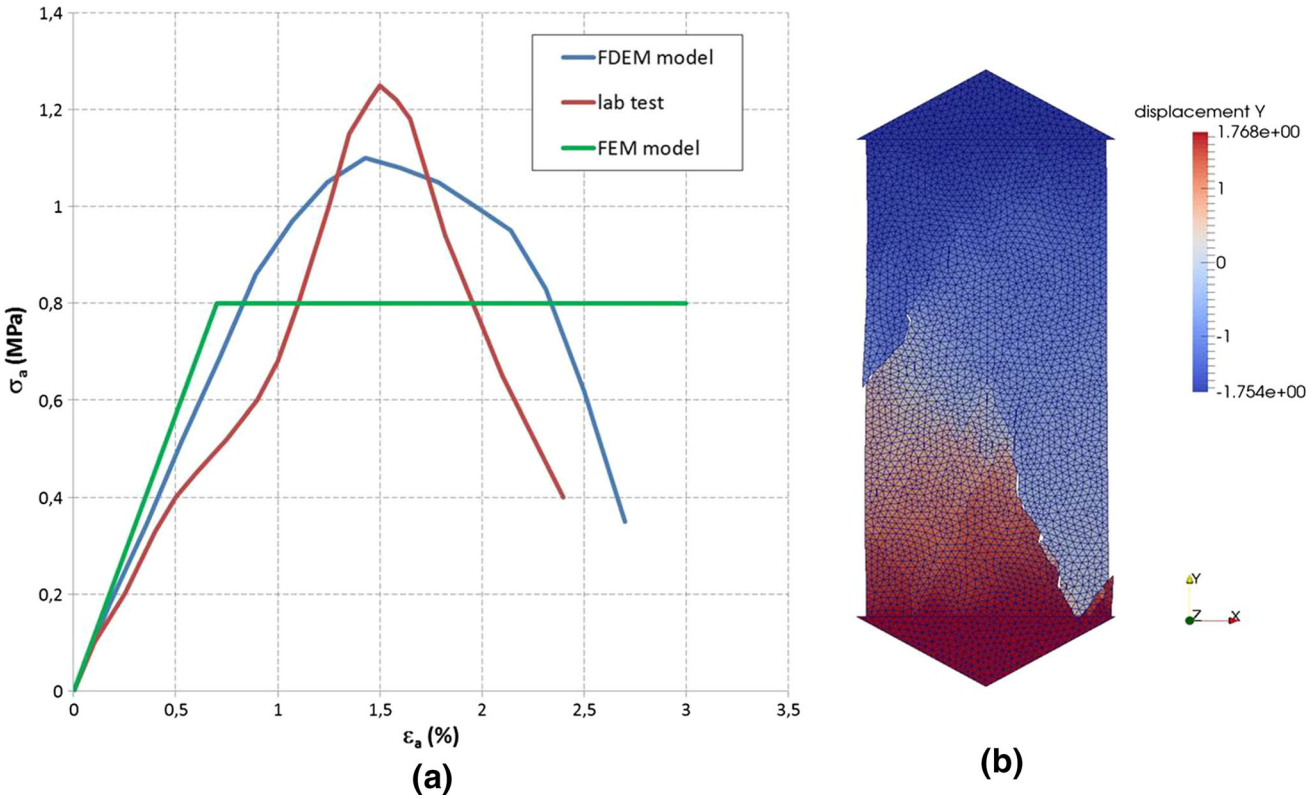

Fig. 10 **a** Uniaxial compression test simulations on a calcarenite sample performed with FDEM and FEM model, as compared with laboratory data; **b** vertical displacement and failure mode obtained from the FDEM test simulation

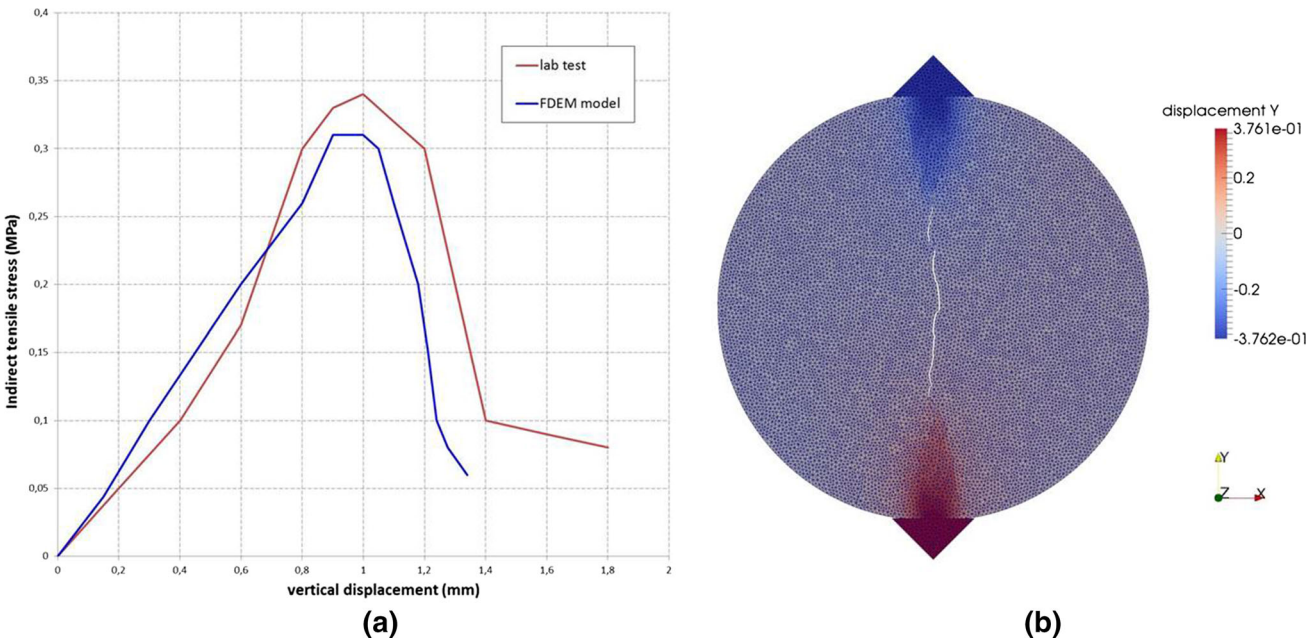

Fig. 11 **a** Indirect tension test simulation on a calcarenite sample performed with FDEM Irazu software compared with laboratory data; **b** vertical displacement and failure mode obtained from the FDEM test simulation

representative, also in terms of geometrical features, of the regions of the Apulian landscape (Southern Italy) where extensive calcarenite deposits crop out. In particular, the FDEM simulations have been performed by accounting for $G_{If} = 20$ N/m–$G_{IIf} = 200$ N/m and $G_{If} = 10$ N/m–$G_{IIf} = 100$ N/m fragility parameters, the latter being

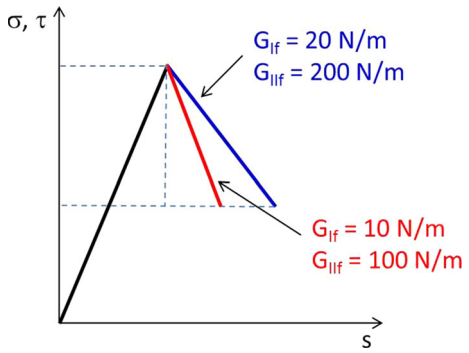

Fig. 12 Schematic representation of the fracture energy parameters adopted

representative of enhanced brittle behaviour (Fig. 12). In order to avoid effects related to the mesh size, FDEM and FEM analyses presented hereafter are characterized by the same mesh size. As below described in detail, a very fine mesh area has been adopted in the area close to the process zone for both the numerical approaches.

4.1 Shallow Underground Cavities

The first ideal problem is represented by the assessment of stability of two shallow underground cavities with rectangular cross section. The geometrical parameters of the first cavity are: width (b) equal to 6 m, height (h) of 4 m and roof thickness (t) of 8 m (Fig. 13a). Gravity loading conditions were firstly assigned to derive the initial stress state in the domain; afterwards, the cavity excavation was simulated in a single stage, which is supposed to represent the most adverse condition for stability. The discretization mesh is formed of a zone around the cavity with 0.4 m size triangular elements and an area far from the cavity with coarser elements. The numerical results obtained from a FEM analysis performed with PLAXIS-2D (2015) in terms of plastic points and deviatoric strains calculated by assuming the mechanical parameters corresponding to *Set 3* of Table 2 are shown, respectively, in Fig. 13b, c. These figures indicate that plastic points develop only along the vertical walls of the cavity and the deviatoric strains follow a wedge shape starting from the apexes of the cavity walls. The calculated horizontal displacements are shown in Fig. 13d and confirm the wedge deformation mechanism, with a maximum value of displacement equal to 3 mm (Fig. 13d). The cavity is stable and the factor of safety (FS), as calculated by means of the strength reduction method, is equal to FS = 1.57.

In order to explore the role of brittleness and fragmentation of the calcarenites, analyses of the same cavity problem were carried out using Irazu FDEM software. The mesh adopted for these analyses is formed of triangular elements 0.4 m size in the area around the cavity, in order to have very small elements as compared with the size of the engineering problem (Fig. 14), as suggested by Munjiza and John (2002), as well as to have a mesh size comparable with that of the FEM analysis. The initial stress state has been assigned by increasing linearly the value of the gravitational acceleration from zero to the final value (i.e. $g = -9.81$ m/s^2) over a large number of time steps in order to reduce the risk of fragmentation due to dynamic oscillations in the model, so that the rock behaviour is

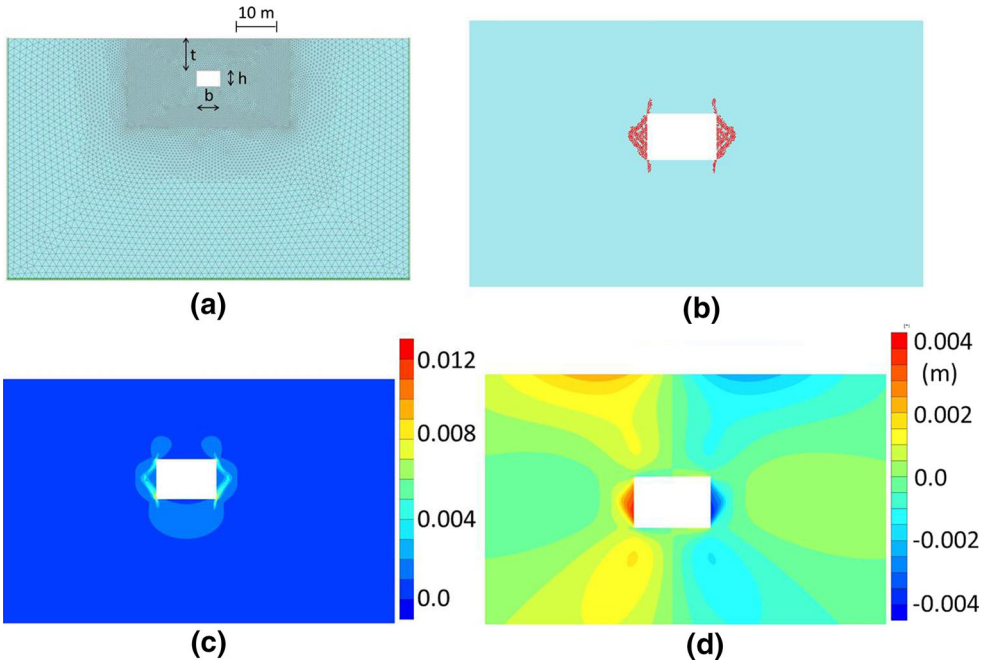

Fig. 13 FEM model of the 6 × 4 m underground cavity: **a** FEM discretization mesh and geometrical parameters, **b** plastic points, **c** deviatoric strains, **d** horizontal displacements

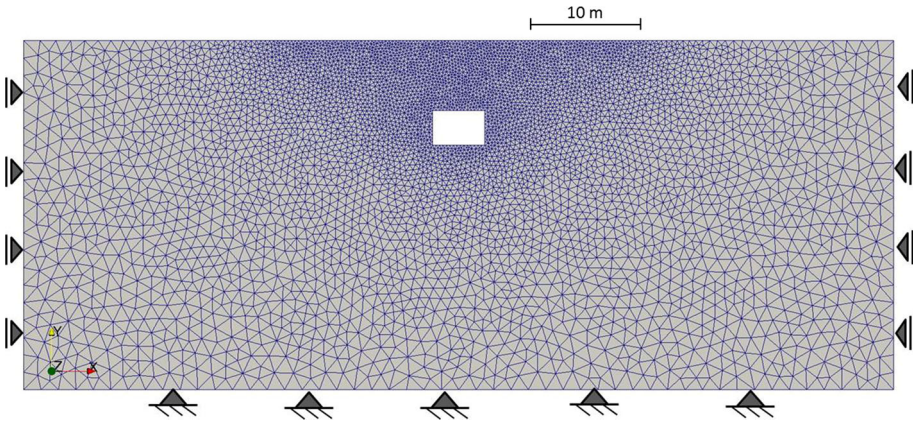

Fig. 14 FDEM model of the 6 × 4 m underground cavity: domain, boundary conditions and discretization mesh

investigated only at the end of the stage under which gravity is increased. The vertical boundaries are fixed only in the *x*-direction, whereas the bottom of the domain has been fixed in both the *x*- and the *y*-direction. The same elastic moduli used for the FEM analysis, i.e. $E' = 100$ MPa and $v = 0.3$, as well as the same Mohr–Coulomb parameter set used for the FEM calculation were implemented in the FDEM analyses. Fracture energy parameters equal to $G_{If} = 10$ N/m and $G_{IIf} = 100$ N/m were used in order to explore the influence of an enhanced brittleness of the rock examined (Fig. 12) on the stability of the cavity. In particular, the corresponding results, shown in terms of horizontal displacement in Fig. 15, indicate that the cavity is globally stable, but highlight local detachments affecting rock portions of variable size along the cavity walls, which suggest typical spalling mechanisms.

A second underground cavity, $b = 16$ m wide and $h = 4$ m high, with a roof thickness (t) equal to 8 m (Fig. 16), was also modelled as a representative highly unstable ideal case, firstly by assuming perfect plasticity (FEM analysis) and secondly by accounting for post-peak brittleness (FDEM analysis). Regarding the FEM model, *Set 2* ($c' = 200$ kPa, $\phi' = 30°$ and $\sigma_t = 180$ kPa) in Table 2 was accounted for to simulate the rock strength. The same numerical procedure was used, as for the previous cavity analysis and the discretization mesh is again characterized by a finer zone around the cavity, with 0.4 m element size (Fig. 16a). The numerical results, in terms of plastic points and tensile failures, are shown in Fig. 16b and indicate that with these strength parameters only localized plastic points develop in the areas close to the cavity vertexes, while tensile failures are calculated in the centre of the cavity roof. Figure 16c instead shows the contours of deviatoric strain calculated with the same analysis and confirm that only localized strains develop in the areas of the cavity vertexes. The cavity is stable and the factor of safety, as calculated by means of the strength reduction method, is equal to 1.55, with the corresponding

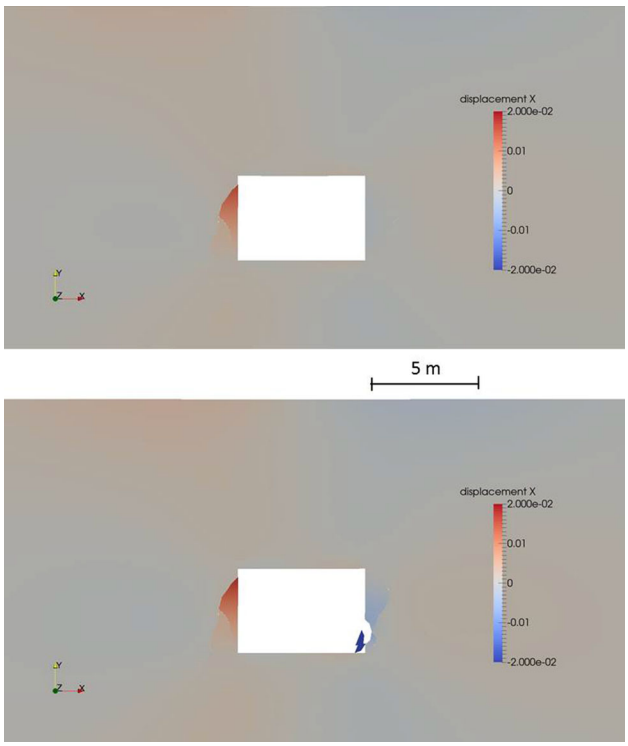

Fig. 15 Horizontal displacements at different time steps obtained from FDEM analysis with $G_{If} = 10$ N/m and $G_{IIf} = 100$ N/m fracture energy parameters

failure mechanism characterized by deviatoric strains that propagate significantly upwards, i.e. towards the ground surface, along the lateral sides of the cavity, thus tending to form a general failure mechanism of the cavity roof (Fig. 16d).

FDEM analyses were also carried out with Irazu software to explore the role that post-failure brittleness can play in the stability of this cavity geometry. The mesh adopted for these analyses is again formed of 0.4 m size triangular elements in a refined area around the cavity (Fig. 17a). The same elastic moduli used for the FEM analysis as well as same Mohr–Coulomb failure parameters

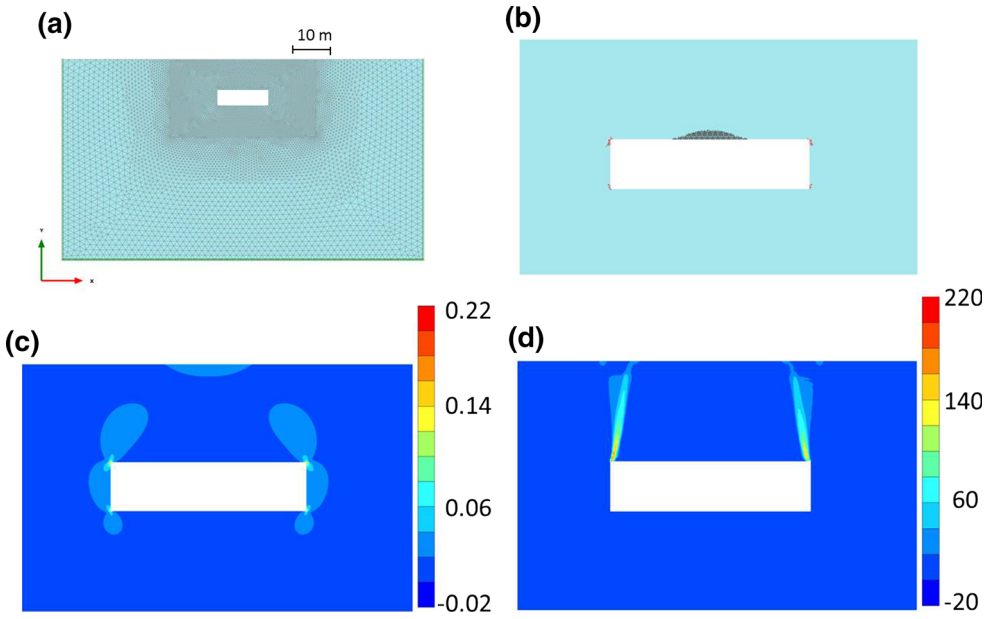

Fig. 16 FEM model of the 16 × 4 m underground cavity: **a** discretization mesh; **b** plastic points (*red points*) and tensile failures (*black squares*); **c** contours of deviatoric strains; **d** contours of deviatoric strains obtained from strength reduction analysis (colour figure online)

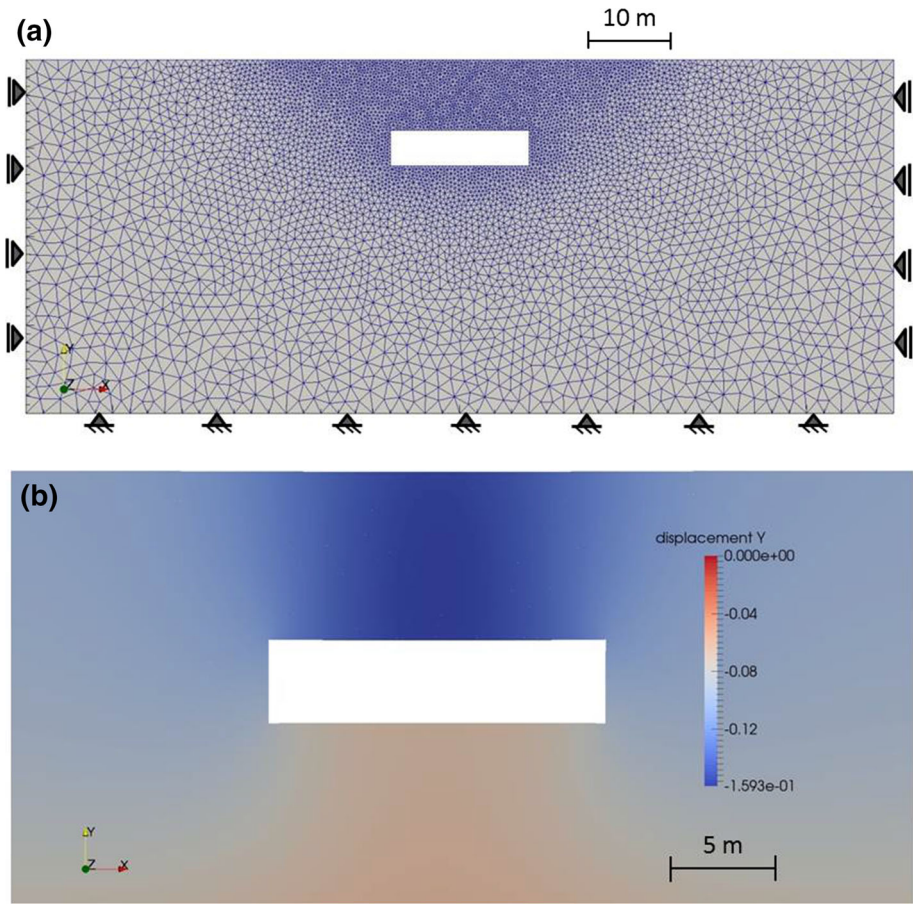

Fig. 17 16 × 4 m cavity FDEM model: **a** discretization mesh; **b** vertical displacements obtained with $G_{If} = 500$ N/m–$G_{IIf} = 5000$ N/m fracture energy parameters

as for the corresponding FEM analysis, i.e. *Set 2* ($c' = 200$ kPa, $\phi' = 30°$ and $\sigma_t = 180$ kPa), were implemented in this FDEM analysis. Using very high fracture energy parameters, i.e. $G_{If} = 500$ N/m and $G_{IIf} = 5000$ N/m, which practically means ductile rock behaviour, the FDEM results indicate that the cavity is stable, although with a concentration of vertical displacements (max value = 15.9 cm) above the cavity roof (Fig. 17b). Later

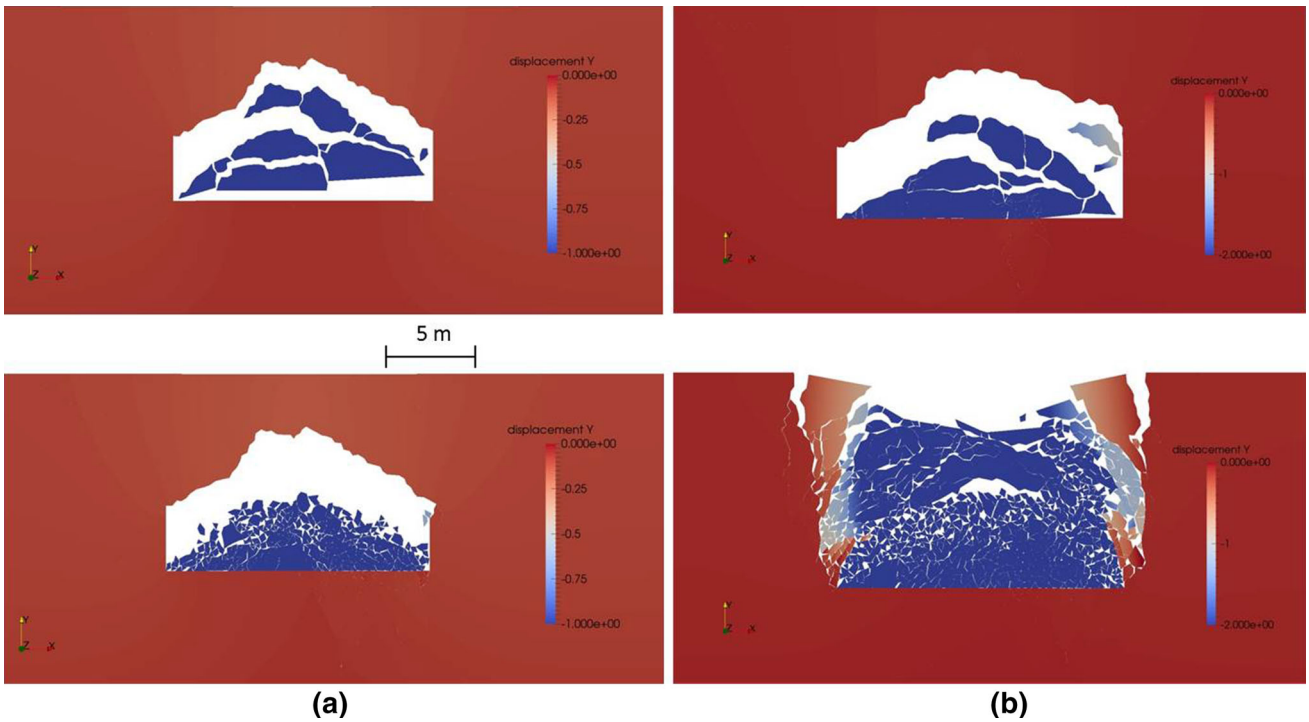

Fig. 18 16 × 4 m cavity FDEM model: vertical displacements obtained with **a** G_{If} = 20 N/m–G_{IIf} = 200 N/m fracture energy parameters; **b** G_{If} = 10 N/m–G_{IIf} = 100 N/m fracture energy parameters

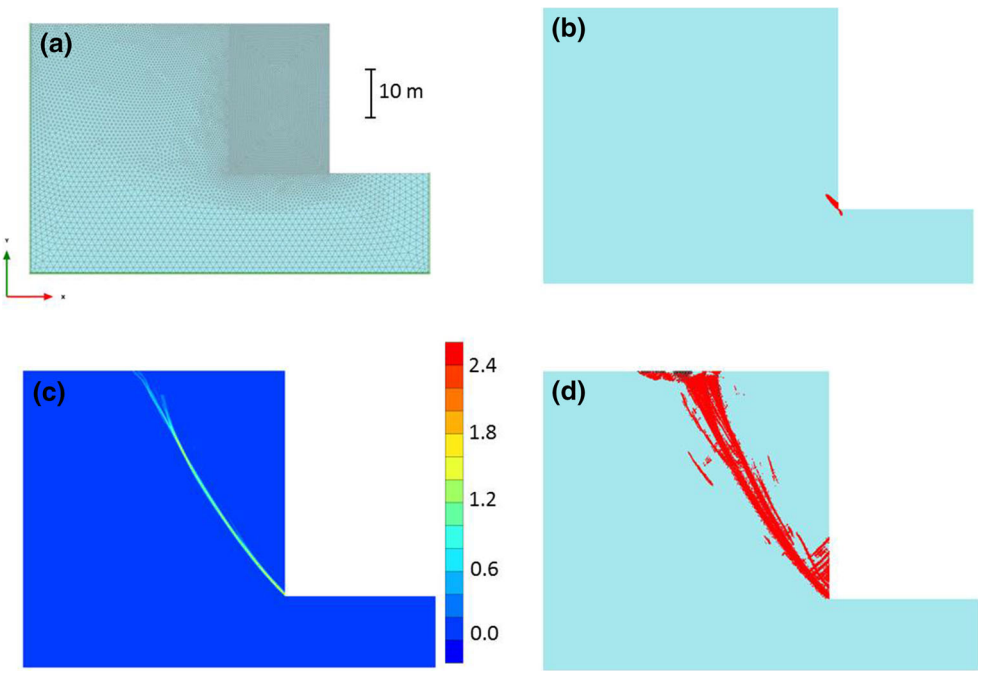

Fig. 19 FEM model of the vertical slope face: **a** discretization mesh; **b** plastic points (*red points*); **c** contours of deviatoric strains; and **d** plastic points (*red points*) and tensile failures (*black squares*) obtained from strength reduction analysis (colour figure online)

on, if fracture energy parameters equal to G_{If} = 20 N/m and G_{IIf} = 200 N/m are implemented, an arch-shaped failure mechanism involving the whole cavity roof, 4–5 m deep, is calculated, although not reaching the ground surface (Fig. 18a). When enhanced brittleness is accounted for, i.e. G_{If} = 10 N/m and G_{IIf} = 100 N/m, failure propagates upwards to the ground surface, thus indicating the generation of a sinkhole, along with enhanced rock fragmentation (Fig. 18b).

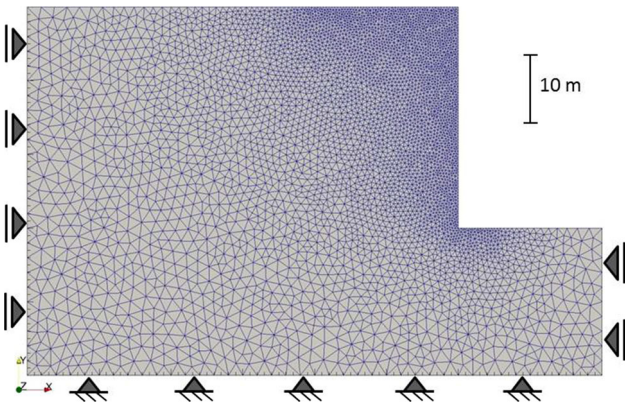

Fig. 20 FDEM model of the vertical slope face: domain, boundary conditions and discretization mesh

4.2 Vertical Rock Slope Face

The second ideal case study here discussed is represented by a 30-m-high vertical slope face (Fig. 19a). Conventional finite element analyses were carried out using a Mohr–Coulomb elastic–perfectly plastic model and implementing the material parameters corresponding to *Set 1* (Table 2). A gravity loading stage analysis was firstly carried out to assign the initial stress state to the calculation domain; a finer discretization mesh, 0.4 m size, has been adopted in the area close to the vertical slope face, whereas a coarser mesh has been used for the areas far from that of interest (Fig. 19a). The corresponding results in terms of plastic points are reported in Fig. 19b and show that only a very limited plastic zone develops at the toe of the vertical slope. The safety factor (SF) calculated by means of the strength reduction method is equal to FS = 1.93, and the corresponding failure mechanism is shown in Fig. 19c, d, respectively, in terms of deviatoric strains and plastic zones, which indicate an inclined failure surface from the toe to the top of the vertical slope.

FDEM analyses were then performed in order to explore the role of calcarenite brittleness also for this type of problem. The mesh adopted for these analyses is also formed of triangular elements of 0.4 m size in the area close to the vertical slope, as for the FDEM cavity analyses (Fig. 20). The same elastic moduli, $E' = 100$ MPa and $\nu = 0.3$, as well as the same Mohr–Coulomb failure parameters used for the FEM analysis were adopted in the FDEM analyses. Different fracture energy parameters, $G_{If} = 20$ N/m–$G_{IIf} = 200$ N/m and $G_{If} = 10$ N/m–

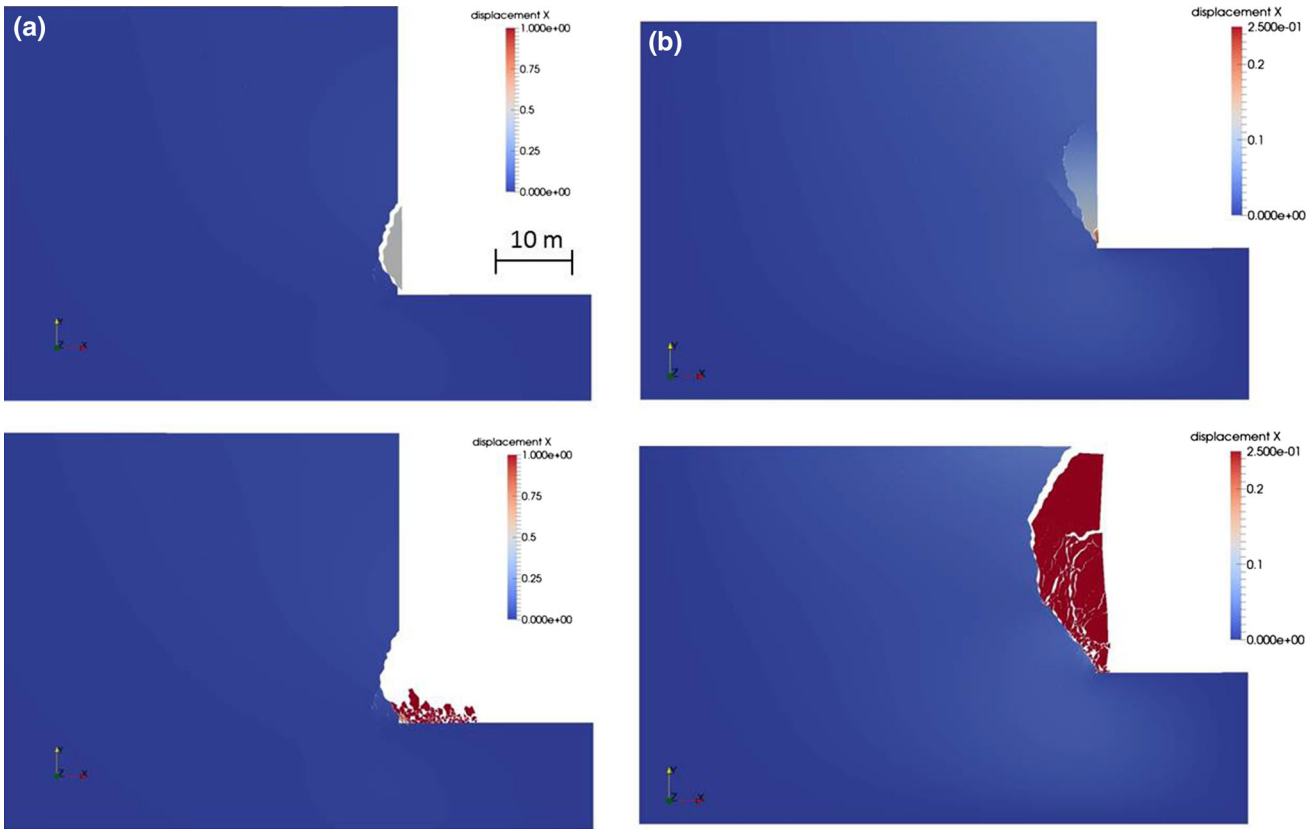

Fig. 21 Vertical slope face FDEM analysis: horizontal displacements obtained with **a** $G_{If} = 20$ N/m–$G_{IIf} = 200$ N/m fracture energy parameters; **b** $G_{If} = 10$ N/m–$G_{IIf} = 100$ N/m fracture energy parameters

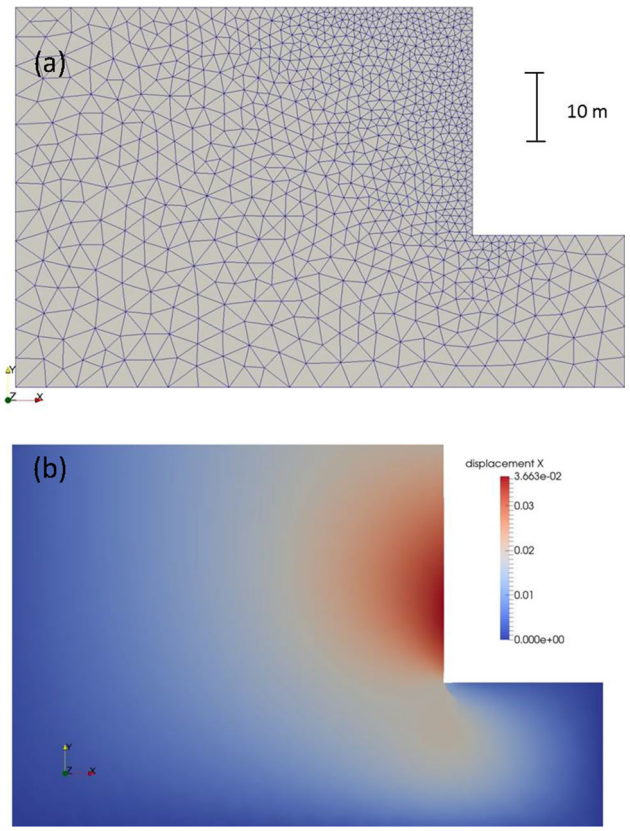

Fig. 22 Vertical slope face FDEM analysis: **a** coarser discretization mesh; **b** horizontal displacements obtained with $G_{If} = 20$ N/m–$G_{IIf} = 200$ N/m fracture energy parameters

$G_{IIf} = 100$ N/m (Fig. 12), were applied to explore the role of these parameters on the slope face stability. The numerical results indicate that when mean brittleness parameters are implemented, i.e. $G_{If} = 20$ N/m and $G_{IIf} = 200$ N/m, the vertical slope is unstable with a local failure mechanism that involves the lower portion of the vertical face, characterized by the detachment of a 3-m thick and 10-m-high arch-shaped slice (Fig. 21a). Figure 21b instead shows the results obtained assuming $G_{If} = 10$ N/m–$G_{IIf} = 100$ N/m as energy fracture parameters and indicates that the slope starts to fail in the lower portion of the vertical face, but later on the failure mechanism propagates upwards and involves also the inner portions of the rock mass for the whole slope height. Finally, the effect of the mesh size has been also investigated in this case, since the same analysis has been run by adopting a coarser discretization mesh in the area close to the vertical slope, characterized by an element size equal to 1 m (Fig. 22a). The corresponding results are shown in Fig. 22b in terms of calculated horizontal displacement and highlight that there is no failure mechanism, thus confirming the prominent role of the mesh size in FDEM analyses.

5 Discussion and Conclusions

The comparison between FEM analyses assuming perfect plasticity rock behaviour and FDEM analyses that implement brittle rock response and explicitly capture fracture and fragmentation processes for some ideal problems has provided insights concerning the stability of soft calcarenite rock masses under low confinement conditions. In particular, the adoption of a perfectly plastic model does not allow for exploring the effects of fracture and fragmentation processes for the rock studied which exhibits clear brittleness under testing. This finding suggests that higher factors of safety can be obtained when brittle behaviour and spalling mechanisms are disregarded for the material under consideration, as is demonstrated by the case studies in this paper. Furthermore, if a moderate to high energy fracture is accounted for by using advanced FDEM calculation techniques, capable of implementing both Mode I and Mode II fracture propagation material behaviour, the rock system can exhibit a clear instability under low confinement as well as a local or general failure mechanism. From this point of view, brittleness of soft calcarenites needs to be properly investigated by means of servo-controlled testing machines, even with ordinary laboratory tests propaedeutic to real application problems. It follows that laboratory testing should not be only limited to the characterization of the peak strength properties of the rock or the elastic stiffness properties, but they should also investigate the brittleness stage of the rock mechanical response. As an alternative, FEM-based perfect plasticity models that implement strength conditions accounting for the average post-peak response might be used as a first approximation.

Furthermore, from an experimental point of view, clear brittleness has been observed for the calcarenite samples subjected to laboratory testing under different stress paths, as for example those produced during uniaxial compression, indirect tensile and direct shear tests. However, some difference has been observed for specific calcarenite facies, which show a variable stress–strain behaviour when the water content of the material changes; in particular, the facies characterized by a packstone texture exhibits brittleness in dry conditions, while a more ductile response is observed when the material is saturated. Such a different behaviour between the two conditions is supposed to be related to the spatial distribution of the calcite cementation, which can be irregular and highly variable for the packstone varieties, as well as to the open pore size distribution which affects the water exchange with the external environment. However, these laboratory observations are considered as preliminary and need to be properly investigated in a future work.

The numerical results presented in this work also need to be properly validated in the future by means of back analyses of real case studies characterized by failure of underground caves or vertical slopes for which the brittle response of the calcarenite is derived from specific laboratory tests carried out on rock samples taken from the same study area.

References

Andriani GF, Walsh N (1998) Caratteri tessiturali e resistenza al taglio diretto di calcareniti tenere e porose. GEAM 93:35–42 **(in Italian)**

Andriani GF, Walsh N (2002) Physical properties and textural parameters of calcarenitic rocks: qualitative and quantitative evaluations. Eng Geol 67:5–15

Andriani GF, Walsh N (2003) Fabric, porosity and water permeability of calcarenites from Apulia (SE Italy) used as building and ornamental stone. Bull Eng Geol Environ 62:77–84

Andriani GF, Walsh N (2007) The effects of wetting and drying, and marine salt crystallization on calcarenite rocks used as building material in historic monuments. Geol Soc Lond Spec Publ 271:179–188

Andriani GF, Walsh N (2010) Petrophysical and mechanical properties of soft and porous building rocks used in Apulian monuments (south Italy). Geol Soc Lond Spec Publ 333:129–141

Azzaroli A (1968) Studi illustrativi della Carta Geologica d'Italia. Formazioni Geologiche. Servizio Geologico d'Italia 1:183–185 **(in Italian)**

Backers T, Stephansson O (2012) ISRM suggested method for the determination of mode II fracture toughness. Rock Mech Rock Eng 45:1011–1022

Bishop AW (1967) Progressive failure—with special reference to the mechanism causing it. In: Proceedings of the geotechnical conference Oslo (Norway), pp 142–150

Borja RJ, Regueiro RA, Lai TY (2000) FE modelling of strain localization in soft rock. J Geotech Geoenviron Eng ASCE 126(4):335–343

Cai M, Kaiser PK (2014) In-situ rock spalling strength near excavation boundaries. Rock Mech Rock Eng 47:659–675

Carranza-Torres C, Alonso E, Alejano LR, Varas F, Fdez-Manin G (2002) Elasto-plastic analysis of deep tunnels in brittle rock using a scaled form of the Mohr–Coulomb failure criterion. In: Hammah et al (eds) Proceedings of the 5th North American Rock mechanics symposium NARMS-TAC, Toronto, pp 283–293

Castellanza R, Nova R (2004) Oedometric tests on artificially weathered carbonatic soft rocks. J Geotech Geoenviron Eng ASCE 30(7):728–739

Cheon DS, Park C, Jung YB, Jeon S (2006) Modeling brittle failure of rock using damage-controlled test. In: Proceedings of the 4th Asian rock mechanics symposium, Singapore

Choquette PW, Pray LC (1970) Geologic nomenclature and classification of porosity in sedimentary carbonates. AAPG Bull 54:207–250

Ciantia MO, Castellanza R (2016) Modelling weathering effects on the mecanical behaviour of rocks. Eur J Environ Civ Eng 20(9):1054–1082

Ciantia MO, Castellanza R, di Prisco C (2015) Experimental study on the water-induced weakening of calcarenites. Rock Mech Rock Eng 48:441–461

Cundall P, Carranza-Torres C, Hart R (2003) A new constitutive model based on the Hoek–Brown criterion. In: Brummer et al (eds) Proceedings of the third international symposium on FLAC and FLAC3D numerical modelling in geomechanics, Sudbury, Canada, Balkema, pp 17–25

De Borst R, Sluis LJ, Muhlhaus HB, Pamin J (1993) Fundamental issues in finite element analyses of localization of deformation. Eng Comput 10(2):99–122

di Prisco C, Imposimato S, Aifantis EC (2002) A viscoplastic constitutive model for granular soils modified according to non local and gradient approaches. Int J Num Anal Methods Geomech 26(2):121–138

Diederichs MS (2003) Rock fracture and collapse under low confinement conditions. Rock Mech Rock Eng 36(5):339–381

Diederichs MS (2007) Mechanistic interpretation and practical application of damage and spalling prediction criteria for deep tunnelling. Can Geotech J 44(9):1082–1116

Dunham RJ (1962) Classification of carbonate rocks according to depositional texture. In: Ham WE (eds) Classification of carbonate rocks—a symposium, vol 1. American Ass Petroleum Geol, Memoir, pp 108–121

Eberhardt E, Stead D, Coggan JS (2004) Numerical analysis of initiation and progressive failure in natural rock slopes: the 1991 Randa rockslide. Int J Rock Mech Min Sci 41(1):69–87

Edelbro C (2010) Different approaches for simulating brittle failure in two hard rock mass cases: a parametric study. Rock Mech Rock Eng 43(2):151–165

Elmo D, Stead D (2010) An integrated numerical modelling-discrete fracture network approach applied to the characterisation of rock mass strength of naturally fractured pillars. Rock Mech Rock Eng 43:3–19

Ferrero AM, Segalini A, Giani GP (2010) Stability analysis of historic underground quarries. Comput Geotech 37:476–486

Fraldi M, Guarracino F (2009) Limit analysis of collapse mechanisms in cavities and tunnels according to the Hoek–Brown failure criterion. Int J Rock Mech Min Sci 46:665–673

Geomechanica Inc (2016) Irazu software, version 2.0 Tutorial Manual

Gesualdo A, Minutolo V, Nunziante L (2001) Local collapse in soft rock bank cavities. J Geotech Geoenviron Eng 127(12):1037–1041

Ghazvinian E, Perras M, Diederichs M, Labrie D (2013) The effect of anisotropy on crack damage thresholds in brittle rocks. In: 47th US Rock Mechanics/Geomechanics Symposium, San Francisco, CA, USA, ARMA 13-503

Golchinfar N (2013) Numerical modeling of brittle rock failure around underground openings under static and dynamic stress loadings. MSc Thesis, Laurentian University, Ontario (Canada)

Gui Y, Bui HH, Kodikara J (2015) An application of a cohesive fracture model combining compression, tension and shear in soft rocks. Comput Geotech 66:142–157

Hajiabdolmajid V, Kaiser PK, Martin CD (2002) Modelling brittle failure of rock. Int J Rock Mech Min Sci 39(6):731–741

Hammah HA, Yacoub T, Corkum B, Curran JH (2008) The practical modelling of discontinuous rock masses with finite element analysis. In: The 42nd US rock mechanics symposium, ARMA, 08-180

Hillerborg A, Modeer M, Petersson PE (1976) Analysis of crack formation and crack growth in concrete by means of fracture mechanics and finite elements. Cem Concr Res 6:773–782

Hudson JA (2014) Comprehensive rock engineering: principles, practice and projects. In: Rock testing and site characterization, vol 3. Elsevier, Amsterdam, p 1001

Hudson JA, Crouch SL, Fairhurst C (1972) Soft, stiff and servo-controlled testing machines: a review with reference to rock failure. Eng Geol 6(3):155–189

Iannone A, Pieri P (1979) Considerazioni critiche sui "Tufi Calcarei" delle Murge. Nuovi dati litostratigrafici e paleoambientali. Geografia Fisica e Dinamica Quaternaria 2:173–186 **(in Italian)**

ISRM (1978) Suggested methods for determining tensile strength of rock materials. Int J Rock Mech Min Sci Geomech Abstr 15(3):99–103

ISRM (1979a) Suggested methods for determining water content, porosity, density, absorption and related properties and swelling and slake-durability index properties. Int J Rock Mech Min Sci Geomech Abstr 16:141–156

ISRM (1979b) Suggested methods for determining uniaxial compressive strength of rock materials. Int J Rock Mech Min Sci Geomech Abstr 16(2):135–140

Kaiser PK, Kim BH (2008) Rock mechanics advances for underground construction in civil engineering and mining. In: Proceedings of KRMS 2008, Seoul, pp 3–16

Kaiser PK, Kim BH (2015) Characterization of strength of intact brittle rock considering confinement-dependent failure process. Rock Mech Rock Eng 48:107–119

Labuz JF, Shah SP, Dowding CH (1985) Experimental analysis of crack propagation in granite. Int J Rock Mech Min Sci Geomech Abstr 22:85–98

Lisjak A, Figi D, Grasselli G (2014) Fracture development around deep underground excavations: insights from FDEM modelling. J Rock Mech Geotech Eng 6:493–505

Lollino P, Martimucci V, Parise M (2013) Geological survey and numerical modeling of the potential failure mechanisms of underground caves. Geosyst Eng 16(1):100–112

Mahabadi OK, Lisjak A, Munjiza A, Grasselli G (2012) Y-Geo: new combined finite–discrete element numerical code for geomechanical applications. Int J Geomech 12:676–688

Martin CD (1997) 17th Canadian geotechnical colloquium: the effect of cohesion loss and stress path on brittle rock strength. Can Geotech J 34(5):698–725

Mateu-Vicens G, Pomar L, Tropeano M (2008) Architectural complexity of a carbonate transgressive systems tract induced by basement physiography. Sedimentology 55:1815–1848

Meng F, Zhou H, Zhang C, Xu R, Lu J (2015) Evaluation methodology of brittleness of rock based on post-peak stress–strain curves. Rock Mech Rock Eng 48:1787–1805

Munjiza A (2004) The combined finite–discrete element method. Wiley, Hoboken

Munjiza A, John NWM (2002) Mesh size sensitivity of the combined FEM/DEM fracture and fragmentation algorithms. Eng Fract Mech 69(2):281–295

Munjiza A, Andrews KRF, White JK (1999) Combined single and smeared crack model in combined finite–discrete element analysis. Int J Num Methods Eng 44(1):41–57

Parise M, Lollino P (2011) A preliminary analysis of failure mechanisms in karst and manmade underground caves in Southern Italy. Geomorphology 134:132–143

Pine RJ, Coggan JS, Flynn ZN, Elmo D (2006) The development of a new numerical modelling approach for naturally fractured rock masses. Rock Mech Rock Eng 39(5):395–419

PLAXIS-2D (2015) User's manual. Plaxis BV, Delft

Pomar L, Tropeano M (2001) The Calcarenite di Gravina Formation in Matera (Southern Italy): new insights for coarse-grained, large-scale, cross-bedded bodies encased in offshore deposits. AAPG Bull 85:661–689

Stead D, Coggan JS, Eberhardt E (2004) Realistic simulation of rock slope failure mechanisms: the need to incorporate principles of fracture mechanics. In: Proceedings of SINOROCK international symposium on rock mechanics: rock characterization, modelling and engineering design methods. Int J Rock Mech Min Sci 41, 446

Stead D, Eberhardt E, Coggan JS (2006) Developments in the characterization of complex rock slope deformation and failure using numerical modelling techniques. Eng Geol 83:217–235

Suchowerska AM, Merifield RS, Carter JP, Clausen J (2012) Prediction of underground cavity roof collapse using the Hoek–Brown failure criterion. Comput Geotech 44:93–103

Tatone BSA, Grasselli G (2015) A calibration procedure for two-dimensional laboratory-scale hybrid finite–discrete element simulations. Int J Rock Mech Min Sci 75:56–72

Troncone A (2005) Numerical analysis of a landslide in soils with strain-softening behaviour. Géotechnique 55(8):585–596

Vasak P, Kaiser PK (1995) Tunnel stability assessment during rockbursts. In: Proceedings 3rd Canadian conference in computer applications in the mineral industry, Montreal, Quebec

Wawersik WR, Fairhurst C (1970) A study of brittle rock fracture in laboratory compression experiments. Int J Rock Mech Min Sci 7:561–575

Zhang ZX (2002) An empirical relation between mode I fracture toughness and the tensile strength of rock. Int J Rock Mech Min Sci 39:401–406

Zhao X, Cai MF, Cai M (2010) Consideration of rock dilation on modeling failure and deformation of hard rocks: a case study of the mine-by-test tunnel in Canada. J Rock Mech Geotech Eng 2(4):338–349